Benha Journal of Applied Sciences (BJAS) **print: ISSN 2356–9751**
Vol. (7) Issue (12) (2022), (17-29) **online: ISSN 2356–976x**
http://bjas.journals.ekb.eg

Synergetic effect of dealuminated kaolin and electric arc furnace slag in the preparation of eco-friendly binders

Ibrahim Hatem*, Mohamed Heikal, MY Nassar, and SM Ibrahim
Chemistry Department, Faculty of Science, Benha University, Benha, Egypt
E-mail: ibrahim.shalaby@fsc.bu.edu.eg

Abstract

The work aims to reuse two different industrial solid wastes (Dealuminated kaolin (DK) and Electric arc furnace slag (EAFS)) in the manufacture of eco-friendly binder. The probability of producing the more durable eco-friendly geo-polymer binders is produced from blending EAFS, and DK solid wastes sections with different dosages of alkaline activator solution. The produced binder was treated at ± 30^{o}C at relative humidity (RH) 98 ± 1 %. Different experimental tests were performed such as, compressive strength, combined water, and free slag content. In addition to instrumental techniques such as XRD, DTA/TGA, SEM and FTIR were performed. DK hindered the formation of micro cracks through EAFS-geopolymer and enhanced the C-S-H formation beside enhanced the durability of the binder matrixes.

Key Words: Geo-polymer, Eco-friendly binder, Dealuminated kaolin, and Microstructure.

1. Introduction:

According to sustainable economic study, cement industry has massive environmental implications, owing to high evolution of CO_2 gas and other connected gases through burning fossil fuels [1]. The global CO_2 emissions ≈2.34 billion tones in 2030 from cement plants only [2]. Currently, green house generation (GHG) emissions from cement industry participate by 8% of total national emissions. Green house generation influences the global warming and climate change with environmental system [3]. Cement industries have several implications on soil, air, water, and health as high concentration of hazardous and heavy metals in soil surrounding cement plants [4], health threatening CO_2, SO_2, NO_X and dust particles [5], and high pH, phosphate, nitrate, turbidity, total dissolved and suspended solids with biological oxygen demand [6], respiratory diseases, and eye irritation with cancer risk [7]. To produce 1 ton of clinker, Cement consumes 1800 MJ of energy [8,9].

Considering the above reasons and more, researchers are interested in finding partial or total alternative cementitious binder materials to reduce CO_2 emission and save energy [10,11]. Geopolymer is an eco-friendly building binder material that produced from alkaline activation of solid wastes containing alumina and/or silica sources [12,13]. The alkali activation technique is carried out through five stages: dissolution, precipitation, reorganization, gelation, and polycondensation [14]. Geo-polymerization of industrial aluminosilicate by-products produce amorphous phase and 3D-inorganic network structure called geopolymer. This network structure based on oxygen bridge connects Si-O tetrahedron and Al-O tetrahedron layers [15,16]. Accumulation of industrial solid wastes, not only leading to economic losses but also are toxic, corrosive, explosive, flammable, infectious. In addition to polluting soil, water, and air which causes harmful problems to humans and the environment [17].

Geopolymers are not only eco-friendly cementitious binders and turn hazardous wastes to treasure but also have many advantages and applications than cement industry. These eco-friendly cementitious binders have great mechanical properties with high strength, fire resistance, artificial ageing resistance, and corrosion resistance [18-22]. They have wide applications in commercial airport, railway and they are used to repair pavement in military bases [23].

In this study we concentrated on Electric Arc France Slag (EAFS) and Dealuminated Kaolin (DK). During the melting process of scrap steel, EAFS can be formed and classified according to lime amount into oxidizing or black slag (lime<40%) and reductive or white slag (lime>40%) [24]. World shift towards steel production from electric arc furnaces (EAF) as low coast and less energy requirements [25]. Around 10% of EAF steel production is EAFS dust [26], which accumulate in the environment and must be recycled to reduce hazardous solid wastes. EAFS is a high oxides source as it contains 25-40% iron oxides, 5–15% aluminum oxides, 10–30% silicon oxides, and 25–40% calcium oxides [27]. EAFS has angular shape, rough surface, and almost crystalline structure [24,28]. Due to high content of iron and iron oxides, its density varied from 3000-3500kg/m^3 [29]. EAFS shows high abrasion and fragmentation resistance [30], high mechanical strength, good workability, and less affected by sulphate and fire attack [31].

Dealuminated kaolin (DK) is a waste from aluminum sulphate industry. Calcination of kaolin at 700-800^{o}C produce high reactive source of alumina/silica pozzolanic material called metakaolin ($Al_2O_3.2SiO_2$). Dissolution of metakaolin (MK) in sulfuric acid produces alum as a main product leaving acidic silica solid waste (DK) [32-36]. During dealumination process, large amount of DK produced (around 50% of total alum production) which disposed in landfills and pollute the surrounding areas [35]. Type of inorganic acid used during dealumination process determine SiO_2/Al_2O_3 ratio and BET value of DK [37,38]. Al and Fe contents of DK decreased as concentration of acid and reaction time increased [38]. Acid leaching for MK increased the surface area of DK up to 92.5 m^2/g, this is due to the formation of the high active amorphous silica structure network. DK has high pozzolanic activity than silica fume itself and ability to fix lime than silica fume and MK [37,39].

Generally, geopolymers have intensive resistance to fire attack due to their Si-O-Al network structure [40]. These binder materials are suitable for fire risk buildings such as tunnels and huge buildings. Unlike Portland cement which begin to disintegrate above 300^{o}C [41], geopolymers exhibit fire resistances up to 1000^{o}C without toxic gas emission or sudden degradation due to their ceramic like properties [42,43]. According to water content, mix composition, and alkaline activator, geopolymer exhibit varied behavior when exposure to temperature above 800^{o}C [44]. Recrystallization, sintering structure, and phase transformation may include this behavior [44]. Geopolymers have application as they can be used as thermal insulator, refractory material, fire protector, sound absorber, and as storage concrete for thermal energy [45-48].

However, there are numerous studies of utilize EAFS as cementitious material and an aggregate in Portland cement system [24,32], there are limited studies concerned on using EAFS as a starting material for geo-polymerization technique. So, we investigate the physio-chemical, mechanical and fire resistance characteristics of EAFS-geopolymer and modify these properties by addition different amount of dealuminated kaolin (DK).

2. Materials and experimental procedures:

2.1. Raw materials:

Electric arc furnace slag (EAFS) was obtained from Ezz-El-Dekhila Steel Company, Alexandra Governorate, Egypt. Dealuminated kaolin (DK) was collected from Egyptian Alum Company, Abou Zaabal, Al Qalyubia Governorate, Egypt.

Dealuminated kaolin (DK) is a byproduct for the manufacture of aluminum sulfate industry from Egyptian kaolin. The chemical composition of these raw materials is summarized in Table 1. Figure 1 represented the particle size distribution of dealuminated kaolin (DK) and electric arc furnace slag (EAFS). Dk participated mainly under size 7µm. The particle size distribution of EAFS have two grain size, more than 40% of particles located under 10 µm and other particles located below 45 µm. The morphology of EAFS and DK were investigated by scanning electron microscope (SEM) as shown in Figure 2 and 3, respectively. The micrograph of EAFS represented a semicrystalline structure with high component of iron and zinc. The microstructure of DK displayed as layered morphology.

Table (1) Chemical composition of starting raw materials: EAFS, D.K and SSL

Oxides, mass%	EAFS	D.K	SSL
SiO_2	4.6	77.70	30.345
Al_2O_3	1.34	5.48	-
Fe_2O_3	22.54	0.66	-
CaO	29.90	0.18	-
MgO	1.03	0.05	-
TiO_2	-	4.25	-
SO_3	-	2.13	-
K_2O	-	0.11	-
Na_2O	-	0.04	14.45
Zn	8.54	-	-
C	1.91	-	-
L.O.I	30	9.10	55.205
Total	97.95	99.99	100

L.O.I: loss of ignition.

Figure 4 represented XRD patterns of EAFS and DK Figure 4 showed the diffraction peaks corresponding to magnesio-ferrite (Fe_2MgO_4), calcite ($CaCO_3$), and rhodonite ($Ca_{0.3}Fe_{0.4}Mg_{0.1}Mn_{4.2}O_{15}Si_5Zn_{0.005}$) phases beside zincite phase (ZnO). The major component of DK is quartz (Q) and little amount is TiO_2 (T) with considerable amorphous structure.

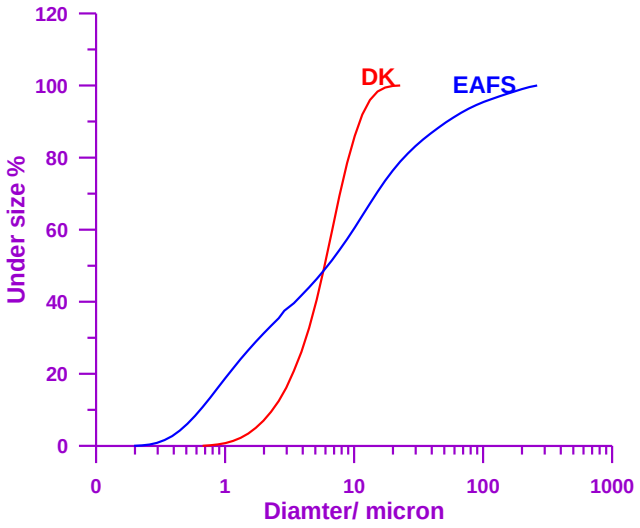

Fig. (1) Size distribution of EAFS and DK

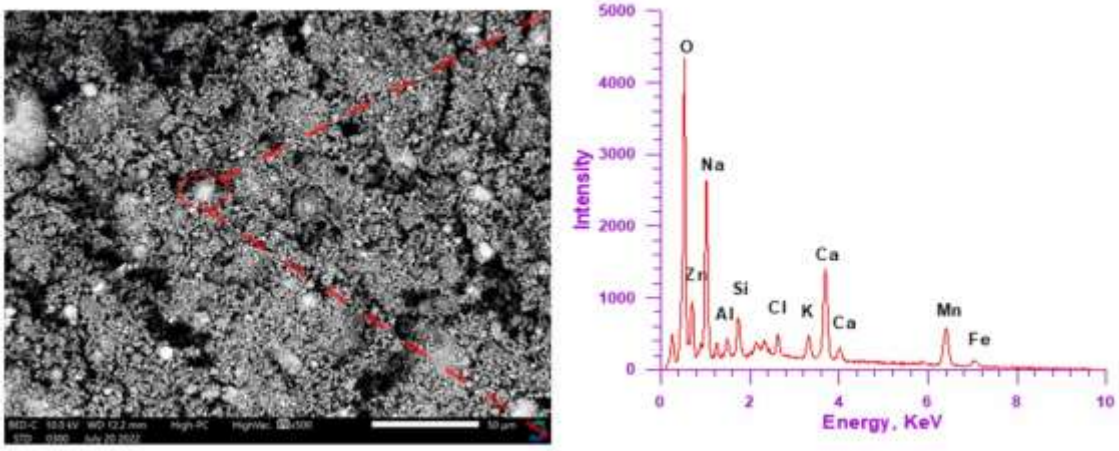

Fig. (2) SEM of EAFS.

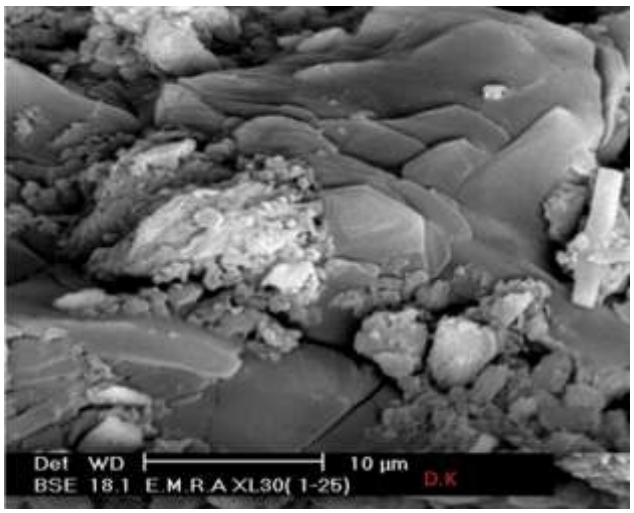

Fig. (3) SEM of DK

The Fourier-transformation infrared spectroscopy (FT-IR) of EAFS are shown in Figure 5. The bands located at 497, 1045, 1402, and 2925 cm^{-1} specific for EAFS and 465, 691, 796, and 1091cm^{-1} for DK which indicated to Si-O and Si-O-Si bonds.

Sodium silicate liquid (SSL) collected from Egyptian Saudi for chemical Industries company, Bader City, Cairo, Egypt. SSL contains 14.45% Na_2O, 30.35% SiO_2, and 55.21% H_2O. Sodium hydroxide pellets 99.8% purity were used as alkali materials for activation process.

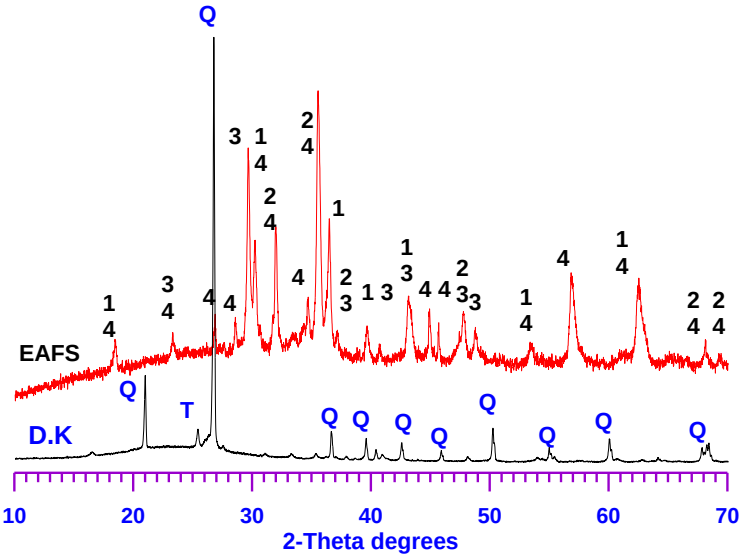

Fig. (4) XRD patterns of EAFS and DK; 1= Magnesio-ferrite (Fe_2MgO_4), 2=Zincate (ZnO); 3=Calcite ($CaCO_3$), 4=Rhodonite ($Ca_{0.3}Fe_{0.4}Mg_{0.1}Mn_{4.2}O_{15}Si_5Zn_{0.005}$), Q=Quartz ($SiO_2$) and T= TiO_2.

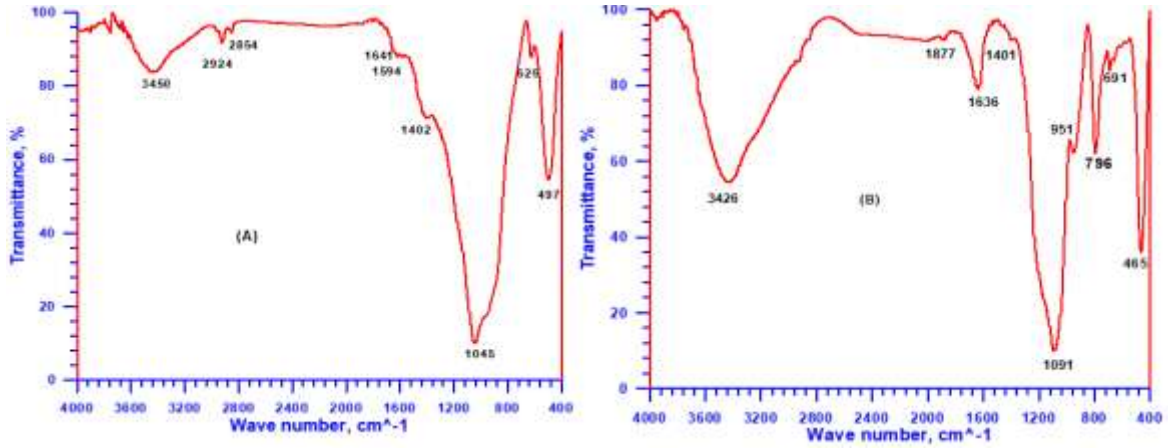

Fig. (5) FTIR spectra of (A) EAFS and (B) DK.

2.2. Preparation of geopolymer binder mixes:

Different concentrations of alkali activator (Na_2O and SSL) were applied to electric arc furnace slag (EAFS) to achieve the optimum mix (1 mol Na_2O and 0.5 mol SSL). Different EAFS/DK geopolymer mixes were prepared by varying the percentages of DK as 10, 20, 30, and 50%. The compositions of these mixes are shown in Table 2. Each mix was blended in a porcelain ball mill for 2hrs in the presence of four balls using a mechanical roller. After mixing, freshly prepared geopolymer was casted into 2×2 cm cylinder molds, then the geopolymer pastes were pressed to obtain homogeneity specimen, then vibrated for 5min in vibrating table. The samples were cured at 30 ^{0}C for 72 hrs. After 72 hrs, the casted molds were de-molded and then the specimens were treated at ± 30^{o}C at humidity cabinet at RH= 98 ± 1 % for all cured time up to 90-days.

Table (2) Composition of prepared geo-polymer mixes.

Mix Abb.	EAFS	D.K	SiO_2, mol/kg	Na_2O, mol/kg	W/S ratio
EAFS1	100	-	0.50	0.50	21
EAFS2	100	-	0.50	0.75	21
EAFS3	100	-	0.50	1.00	22
EAFS4	100	-	0.50	1.50	23
EAFS3.DK1	90	10	0.50	1.00	24
EAFS3.DK2	80	20	0.50	1.00	26
EAFS3.DK3	70	30	0.50	1.00	30
EAFS3.DK4	50	50	0.50	1.00	37

2.3 Investigation methods:

Compressive strength was determined for 3 samples according to the ASTM designation (ASTM C109M 2016) [49]. After desert time 3, 7, 14, 28, and 90-days, the hydration of geopolymer binders was stopped using 1:1methanol–acetone mixture, then dried at 70°C for 2h. The stopped specimens were stored in desiccators [50]. Free slag content was determined according to the following reference [51].

The Fourier-transform infrared (FT-IR) spectra were recorded for some selected samples using Genesis FT-IR spectrometer in the range 400-4000 cm^{-1} after 256 scans at 2 cm^{-1} resolution.

The scanning electron microscope (SEM) with an energy-dispersive X-ray analyzer (EDX) was investigated with Inspect S (FEI Company, Holland). The X-ray diffraction patterns (XRD) was applied to the selected samples with the aid of BRUXER, Axis D8 ADVANCE A8, and a Germany diffractometer between 10° and 70° 2-theta and a scanning speed of 1°/min

Thermal gravimetric analysis (TGA/DTG) was applied by using DTA–50 thermal analyzers (Shimadzu Co., Tokyo, Japan) under N_2 gas atmosphere. A dried sample was detected at a heating rate of 10°C/min.

3. Results and Discussion:

3.1. Compressive strength:

The compressive strength of hardened geo-polymer mixes cured at 98 ± 1% RH humidity up to 90 days. Figure 6 shows an increase in compressive strength for all mixes with curing time. For EAFS-geopolymer binder, EAFS3 mix shows the higher values of compressive strength at all hydration-curing time (Figure 6A).

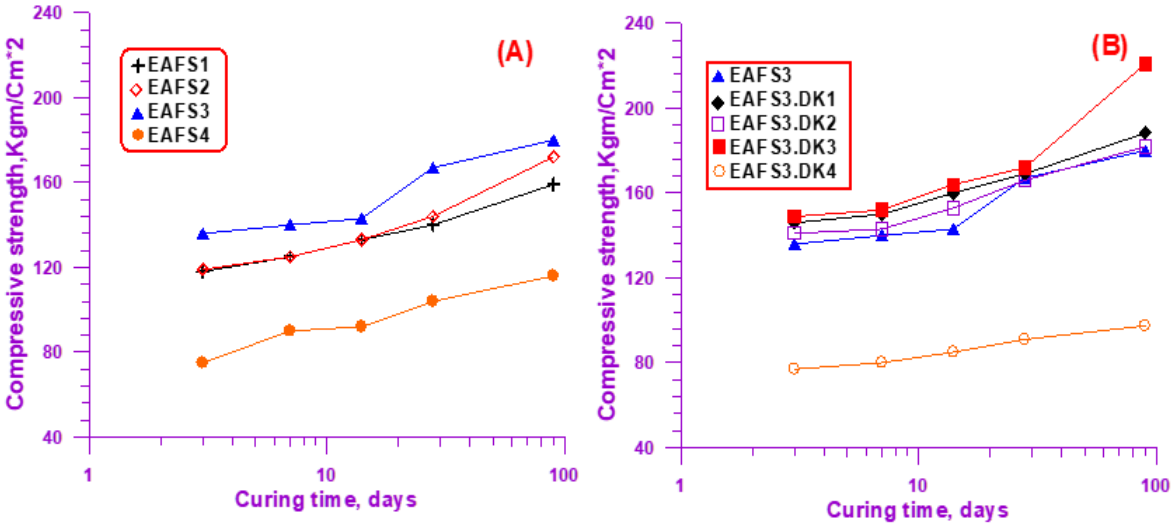

Fig. (6) Compressive strength of alkali activated (A) EAFS mixes and; (B) EAFS3.DK mixes.

Increase of the alkaline activation (Na_2O content) leading to an increase in compressive strength due to high quantity of hydroxyl groups that reacted with Ca^{2+}, Fe^{2+}, and Mg^{2+} cations. Acceleration this reaction by alkali content accelerates the geo-polymerization process and forms high freshy hardened paste in short time producing CSH, CAH, and N(C)ASH (geopolymer gel-cementitious binders). The further increase in alkali content does not influence the activation process but also reduce the compressive strength as represented in EAFS4 mix (1.5 mol Na_2O). This is due to low amorphous character value of EAFS structure and reduction level of long-range structural products as well as increase the porosity of the geopolymer gel matrix, therefore the compressive strength will decrease. High crystalline structure of EAFS produced through air cooling after iron melting process that prevent affected by the high alkaline activation (Na_2O content).

The compressive strength values of hardened geo-polymer EAFS3.DK mixes cured at 90-days are illustrated in Figure 6B. Increase of the content of DK increases the compressive strength value up to 30% DK. The high surface area of amorphous silica contenting the DK (92.5 m^2/g), enhances the formation of CSH, CAH, and N(C)ASH (geopolymer gel), that increases the hardening and strength of geopolymer gel binder formed. For EAFS3.DK geo-polymer mixes (Figure 6B), EAFS3.DK3 (30% DK) shows the highest compressive strength value of all mixes during curing period. Increase of the content of DK up to 50% (EAFS3.DK4 mix), the values of compressive strength decreased as the amount of CSH, CAH, and N(C)ASH gel binders was reduced.

3.2. Combined water content:

Chemically combined water content of EAFS and EAFS3.DK mixes cured up to 90 days are graphically represented in Figure 7. Combined water content (Wn%) is related to the amount of hydration products and degree of polymerization process of geopolymer binders. Deposal of hydrated products in the open pores through continuous hydration leading to increase in combined water contents with curing time. At 7 days, the chemically combined water content for EAFS1, EAFS2, EAFS3, and EAFS4 mixes were 11,82%, 12.06%, 12.32%, and 12.51, respectively. As the Na_2O% content of alkaline activator increased, the partially hydration products increased leading to an increase in chemically combined water contents at 90-days. The Wn content for these mixes were 15.24%, 15.09%, 16.71%, and 15.74% respectively. As the hydration time increased, the hydraulic properties of EAFS increased with the increase in chemically combined water contents.

Figure 7B shows that addition of DK decreases the Wn% content. High pozzolanic activity and high silica source of DK enhance the formation of CSH, CAH, and N(C)ASH (geopolymer gel) with lower water content during curing time [39]. At 90-days, the water content of EAFS3.DK3 was 13.46% while the EAFS3, EAFS3.DK1, EAFS3.DK2, and EAFS3.DK4 were 16.71, 16.11, 14.96, and 13.6, respectively. The mix containing 30% of DK is the optimum addition to maintain and enhance the formation of C-S-H bonds with low value of Wn compared to other mixes [39].

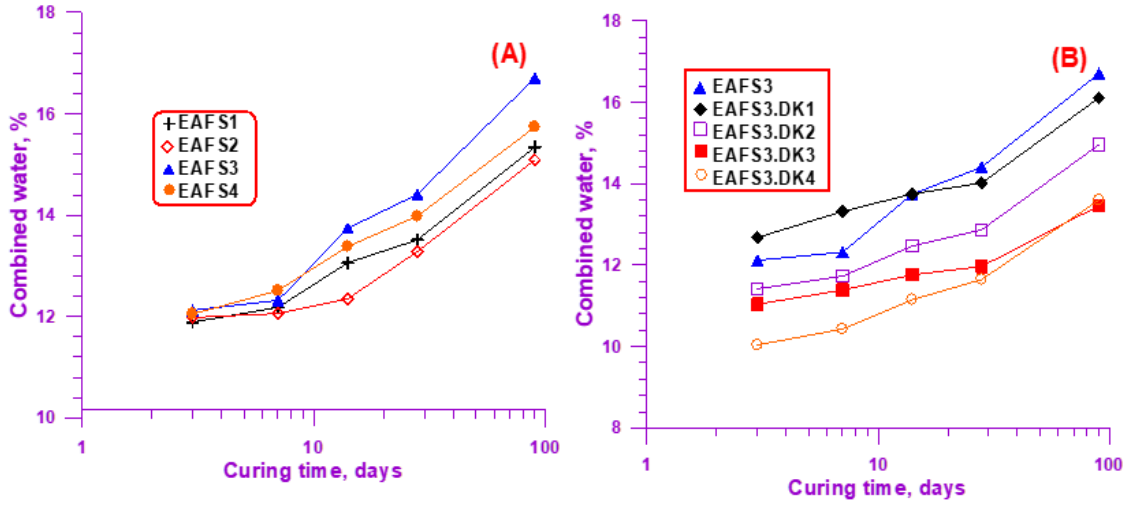

Fig. (7) The chemically combined water contents of alkaline activation of EAFS mix (A), and EAFS3.DK (B).

3.3. Free slag content:

Figure 8 represented the free slag content of EAFS mixes, and EAFS3.DK- geopolymer mixes up to 90 days. For EAFS mixes (Figure 8A), free slag content degreases with increasing alkaline solution. Increasing in alkalinity, increases the hydroxyl ion concentration, hence the concentration of -Si-OH, =Fe-Si-OH, and =Al-Si-OH groups increase. These groups condensed to form crosslinked network structure and free active pozzolana decrease with increasing alkalinity. Free slag content decreased with curing time as the hydrated products increased with time, leading to the free active pozzolana content decreased.

Addition of DK (Figure 8B) increases the initial free slag content as DK is high reactive source of free pozzolanic activity = 85% comparting to EAFS= 56%. The free slag content for EAFS3, EAFS3.DK1, EAFS3.DK2, EAFS3.DK3, EAFS3.DK4 at 3days were 48.88%, 63.82%, 61.44%, 69.58%, and 78.32%, respectively, whereas, at 90 days were 37.00%, 53.22%, 49.96%, 59.44%, and 70.60% respectively. With increasing in hydration time, hydration products increase with decreases in free slag content.

3.4. X- ray diffraction patterns:

Figure 9A and B represented the x-ray diffraction patterns of alkaline activated EAFS3 and EAFS3.DK3 geopolymer binder mixes hydrated at 7,28, and 90-days. The x-ray diffraction patterns show the presence of calcium hydroxide (CH) phase at diffraction lines at 4.92, 2.62, 1.92 and 1.79Å for specimens cured at 7 days. The diffraction lines intensity of CH decrease with curing time, this is due to the formation of new additional products namely CSH gel binders. These diffraction detection peaks at all curing ages (7-90 days) associated with formation of CSH-gel overlapping with $CaCO_3$ [50]. New phase zoisite phase ($Al_{2.884}Ca_2Fe_{0.116}HO_{13}Si_3$) is generated during curing time of 28 and 90 days. High crystalline peaks were observed form 2-theta = 28^o to 37^o that evidence to the crystallinity structure of EAFS, which affected on geo-polymerization process. It was noted that magnesio-ferrite (Fe_2MgO_4), and Rhodonite ($Ca_{0.3}Fe_{0.4}Mg_{0.1}Mn_{4.2}O_{15}Si_5Zn_{0.005}$) phases are also present in the diffraction lines [52].

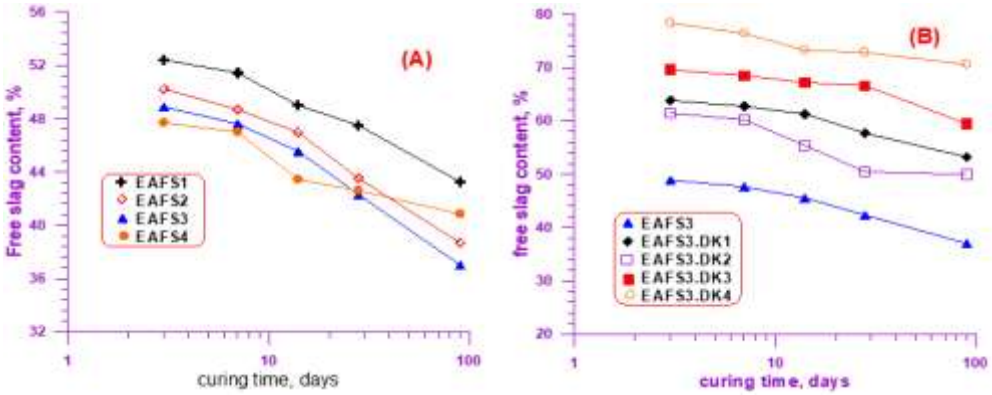

Fig. (8) Free slag content of alkaline activation EAFS mixes (A), and EAFS3.DK mixes (B).

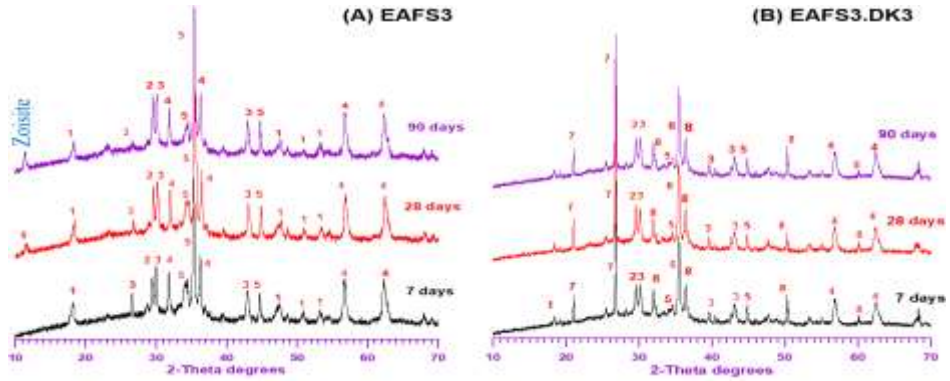

Fig. (9) X-ray diffraction of EAFS3 cured up to 90 days; 1=calcium hydroxide, 2=calcium silicate hydrate, 3= calcite ($CaCO_3$), 4= Magnesio-ferrite (Fe_2MgO_4), 5= Rhodonite ($Ca_{0.3}Fe_{0.4}Mg_{0.1}Mn_{4.2}O_{15}Si_5Zn_{0.005}$), 6=di sodium calcium silicate (Na_2CaSiO_4), 7=quartz (SiO_2), 8= Dialuminium silicate oxide (Al_2SiO_5).

The x-ray diffraction patterns for EAFS3.DK3 represented in Figure 9B. It shows that calcium hydroxide diffraction lines decreased sharply and closely disappear after addition DK to EAFS. The diffraction patterns showed the presence of disodium calcium silicate (Na_2CaSiO_4), di aluminum silicate oxide (Al_2 Si O_5), and quartz which enhance the formation of CSH, CASH, and N(C)SH gel formation. DK acting as a nucleation center for generation and accumulation of geopolymers [40] that has appositional affect in compressive strength (Figure 6B) and morphology structure as shown later in Figure 12.

3.5. TGA/DTA thermograms:

Figure 10A and B represented the TGA/DTG thermograms of EAFS3, and EAFS3.DK3-geopolymer mixes cured at 7, 28 and 90 days. Free water, adsorbed water, water content of N(C)ASH, CSH, and CAH related phases removed at endothermic peaks ≥200°C. Endothermic peak at 480°C is related to presence of $Ca(OH)_2$ as well as endothermic peaks from 600°C to 800°C is related to decomposition of calcite [53].

At 800°C, the weight losses of EAFS3 mix were 11.85%, 15.29%, and 16.31% for 7, 28, and 90days respectively. Increasing of weight loss with curing stages associated with geo-polymerization process. Below 200°C the weight losses of EAFS3 mix were 2.22%, 3.15%, and 3.56% which indicate that the amount of N(C)ASH, CSH, and CAH geopolymer gel binders increased with the curing ages up to 90-days. Figure 10A shows the decreasing in the intensity of peaks at 480°C with time that related to the decomposition of calcium hydroxide (CH) due to the formation of more hydrated products (CSH, N(C)ASH, and CASH) in addition to the transformation of $Ca(OH)_2$ to calcium carbonate with time [52]. This endothermic peak disappeared after the addition of DK in the EAFS3.DK mixes, due to reactivity of DK, which enhanced the geo-polymerization process as shown in Figure 10B.

EAFS3.DK3 shows two main losses of weight (Figure 10B). The first one is located under ≥200°C which indicated to decomposition of free water and high intensity of CSH, CASH, and N(C)ASH gel. The weight losses ≥200°C of EAFS3.DK3 mix were 4.27%, 4.24%, and 4.66%, these data indicated that the amount of CASH, CSH, and N(C)ASH geopolymer gel binders increased with the curing ages up to 90-days. The second location between 600°C to 800°C which indicated to decomposition of calcite phases.

Addition of DK exhibits the higher weight losses below 200°C than those of EAFS3 mix that conforming the higher compressive strength obtained than EAFS3. On the one hand, EAFS3.DK3 mix exhibited the lower weight losses between 600°C to 800°C than EAFS3 mix compliant to the reduction amount of calcite phase. The endothermic peak at 650°C is related to the decomposition of less crystalline calcite phase. On the other hand, the endothermic peak 700-850°C is related to the decomposition of crystalline calcite phase. While the exothermic peak is characterized by decomposition of CSH phase, which is formed from the pozzolanic reaction, forms the crystalline monocalcium silicate (wollastonite) [54].

3.6. Scanning electron microscopy and EDX:

Figures 11 and 12 showed the SEM images of alkali activated mixes (EAFS3 and EAFS3.DK3) at 7, 28, and 90-days. SEM morphology represented the existence of high crystalline structure with many voids and unreacted particles of EAFS (Figure 11). The SEM showed formation of calcium silicate hydrate (CSH, CAH, CASH, and N(C)ASH geopolymer gel) on the surface of EAFS grains, which its intensity partially increased with curing time. At 28 days, heterogenous distribution of geopolymer particles was observed on the surface of EAFS grains. At later age (90 days), some crystalline structure of CSH, CAH, CASH, and N(C)ASH geopolymer gel were observed which take leaves structure. This morphology enhanced the compressive strength development as illustrated in Figure 6.

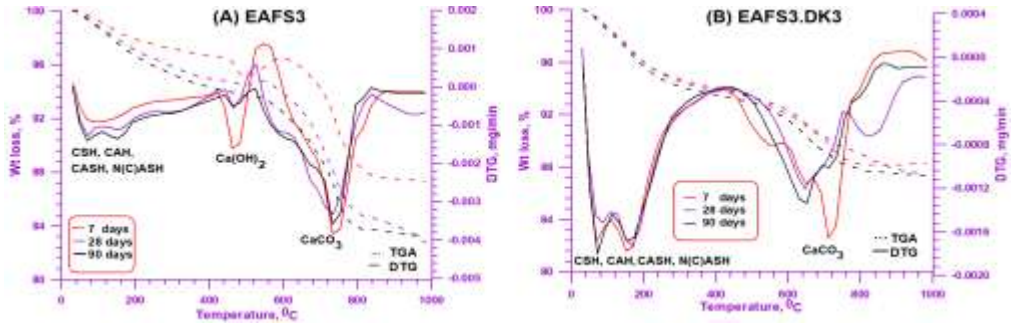

Fig. (10) TGA/DTG of alkaline activation EAFS3 mix (A); and EAFS3.DK3 mix (B) cured at 7, 28 and 90 days.

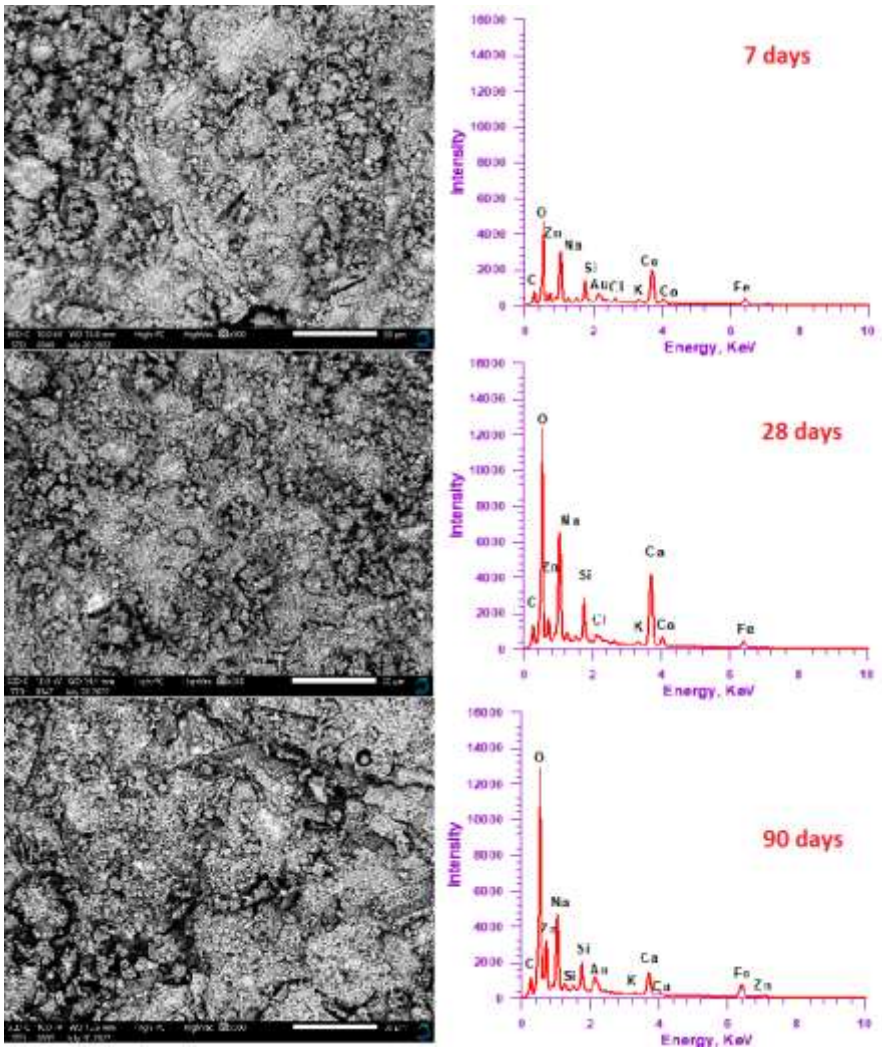

Fig. (11) SEM and EDX of alkali activated EAFS3-mix after 7, 28, and 90days.

Addition of DK generated massive amount of hydrated products (CSH, CAH, CASH, and N(C)ASH) which distributed homogeneity on the surface of EAFS particles. Voids and pores, which located within the micrographs (Figure 11) of EAFS were filled as depicted in Figure 12, producing a closed-dense and uniform matrix structure [34]. Incorporation of DK enhanced the formation of the distinct CSH, CAH, CASH, and N(C)ASH gel-structure associated with alkali activation process, due to high rich of reactive silica and alumina sources containing the DK particles. At 90 days, dense fibrous structure of CSH, CAH, and CASH were formed as well as a nucleation center to N(C)ASH gel matrix to form compact microstructure. These compact microstructures enhanced the compressive strength of geopolymer binder [50]. EDX confirmed that the major hydrated products were CSH, CASH and N(C)ASH which intensity increases with curing time.

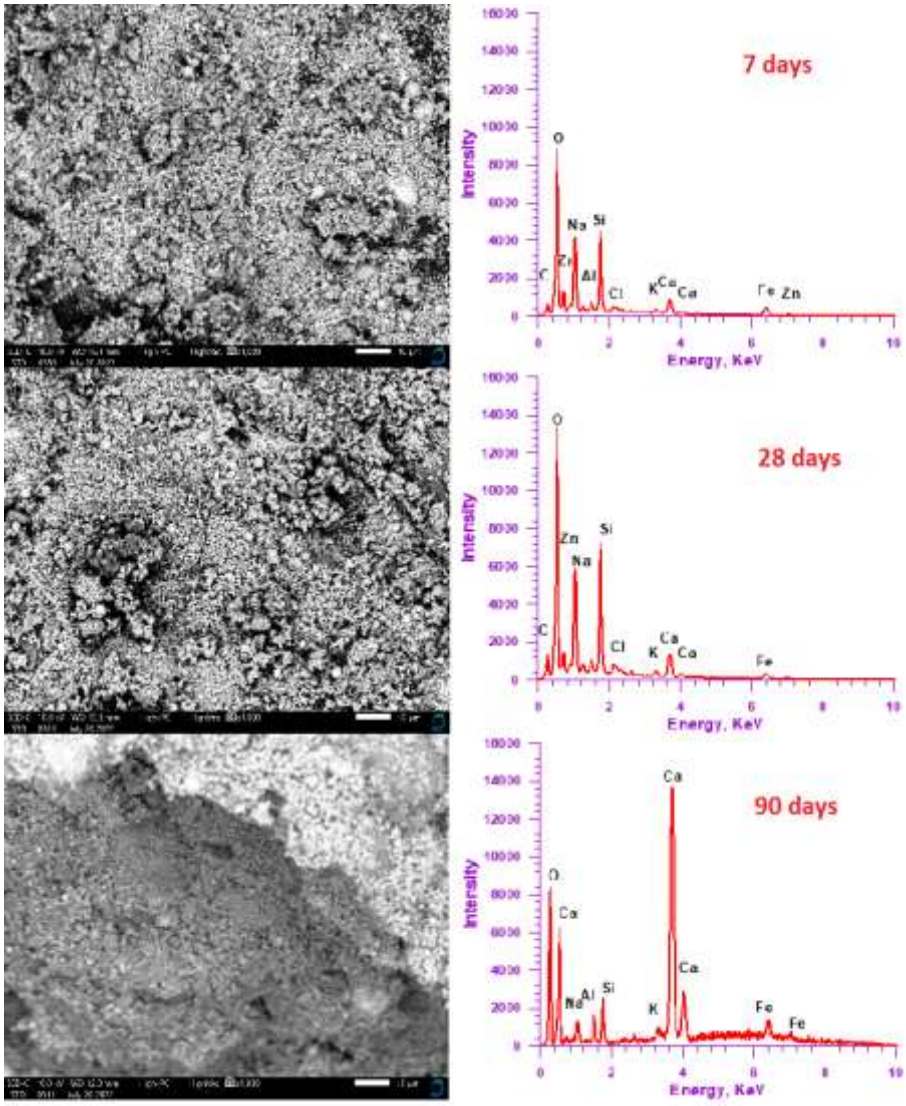

Fig. (12) SEM and EDX of alkali activated EAFS3.DK3-geopolymer mix after 7, 28, and 90days.

4. Conclusions

The main conclusions are:

1. Increase of the alkaline activation of EAFS up to 1.0% Na_2O content leading to an increase in compressive strength. The further increase in alkali content up to 1.5 mol of Na_2O the compressive strength was reduced. Increase of the content of DK increases the compressive strength value up to 30% DK (mix EAFS3.DK3).
2. Increasing alkaline solution increase the chemically combined water as high formation of hydrolytic products.
3. EAFS3.DK3 mix exhibits the higher weight losses ≥200°C than those of EAFS3 mix that conforming the higher compressive strength obtained than EAFS3.
4. DK enhances the formation of the distinct CSH, CAH, CASH, and N(C)ASH gel-structure associated with alkali activation process, due to high rich of reactive silica and alumina sources containing the DK particles. DK hindered the formation of micro cracks through EAFS-geopolymer and enhanced the C-S-H formation beside enhanced the durability of the binder matrixes.

References

[1] Mishra UC, Sarsaiya S, Gupta A. A systematic review on the impact of cement industries on the natural environment. Environmental Science and Pollution Research. 2022:1-12.

[2] Benhelal E, Shamsaei E, Rashid MI. Challenges against CO2 abatement strategies in cement industry: A review. Journal of Environmental Sciences. 2021;104:84-101.
[3] Balsara S, Jain PK, Ramesh A. An integrated approach using AHP and DEMATEL for evaluating climate change mitigation strategies of the Indian cement manufacturing industry. Environmental pollution. 2019;252:863-78.
[4] Kolo MT, Khandaker MU, Amin YM, Abdullah WHB, Bradley DA, Alzimami KS. Assessment of health risk due to the exposure of heavy metals in soil around mega coal-fired cement factory in Nigeria. Results in physics. 2018;11:755-62.
[5] Jokar Z, Mokhtar A. Policy making in the cement industry for CO2 mitigation on the pathway of sustainable development-A system dynamics approach. Journal of Cleaner Production. 2018;201:142-55.
[6] Ipeaiyeda A, Obaje G. Impact of cement effluent on water quality of rivers: A case study of Onyi river at Obajana, Nigeria. Cogent Environmental Science. 2017;3(1):1319102.
[7] Raffetti E, Treccani M, Donato F. Cement plant emissions and health effects in the general population: a systematic review. Chemosphere. 2019;218:211-22.
[8] Abdul-Wahab SA, Al-Rawas GA, Ali S, Al-Dhamri H. Assessment of greenhouse CO2 emissions associated with the cement manufacturing process. Environmental Forensics. 2016;17(4):338-54.
[9] Rashad AM, Zeedan SR. The effect of activator concentration on the residual strength of alkali-activated fly ash pastes subjected to thermal load. Construction and Building Materials. 2011;25(7):3098-107.
[10] Heikal M, Ibrahim SM. Characteristics and durability of alkali activated slag-microsilica pastes subjected to sulphate and chloride ions attack. Ceramics–Silikáty. 2015;59(2):81-9.
[11] Amin M, El-Gamal S, Abo-El-Enein S, El-Hosiny F, Ramadan M. Physico-chemical characteristics of blended cement pastes containing electric arc furnace slag with and without silica fume. HBRC journal. 2015;11(3):321-7.
[12] Cong P, Cheng Y. Advances in geopolymer materials: A comprehensive review. Journal of Traffic and Transportation Engineering (English Edition). 2021;8(3):283-314.
[13] Ren B, Zhao Y, Bai H, Kang S, Zhang T, Song S. Eco-friendly geopolymer prepared from solid wastes: A critical review. Chemosphere. 2021;267:128900.
[14] Nath S, Mukherjee S, Maitra S, Kumar S. Kinetics study of geopolymerization of fly ash using isothermal conduction calorimetry. Journal of Thermal Analysis and Calorimetry. 2017;127(3):1953-61.
[15] Wan Q, Rao F, Song S, García RE, Estrella RM, Patino CL, et al. Geopolymerization reaction, microstructure and simulation of metakaolin-based geopolymers at extended Si/Al ratios. Cement and Concrete Composites. 2017;79:45-52.
[16] Hu S, Zhong L, Yang X, Bai H, Ren B, Zhao Y, et al. Synthesis of rare earth tailing-based geopolymer for efficiently immobilizing heavy metals. Construction and Building Materials. 2020;254:119273.
[17] Wang W, Zhao Y, Bai H, Zhang T, Ibarra-Galvan V, Song S. Methylene blue removal from water using the hydrogel beads of poly (vinyl alcohol)-sodium alginate-chitosan-montmorillonite. Carbohydrate polymers. 2018;198:518-28.
[18] Gökçe H, Tuyan M, Nehdi M. Alkali-activated and geopolymer materials developed using innovative manufacturing techniques: A critical review. Construction and Building Materials. 2021;303:124483.
[19] Amran YM, Alyousef R, Alabduljabbar H, El-Zeadani M. Clean production and properties of geopolymer concrete; A review. Journal of Cleaner Production. 2020;251:119679.
[20] Shuai Q, Xu Z, Yao Z, Chen X, Jiang Z, Peng X, et al. Fire resistance of phosphoric acid-based geopolymer foams fabricated from metakaolin and hydrogen peroxide. Materials Letters. 2020;263:127228.
[21] Liu Y, Su P, Li M, You Z, Zhao M. Review on evolution and evaluation of asphalt pavement structures and materials. Journal of Traffic and Transportation Engineering (English Edition). 2020;7(5):573-99.
[22] Abdel-Ghani NT, Elsayed HA, AbdelMoied S. Geopolymer synthesis by the alkali-activation of blastfurnace steel slag and its fire-resistance. Hbrc Journal. 2018;14(2):159-64.
[23] Shill SK, Al-Deen S, Ashraf M, Hutchison W. Resistance of fly ash based geopolymer mortar to both chemicals and high thermal cycles simultaneously. Construction and Building Materials. 2020;239:117886.

[24] Rashad AM. A synopsis manual about recycling steel slag as a cementitious material. Journal of Materials Research and Technology. 2019;8(5):4940-55.
[25] Jiang Y, Ling T-C, Shi C, Pan S-Y. Characteristics of steel slags and their use in cement and concrete—A review. Resources, Conservation and Recycling. 2018;136:187-97.
[26] Bignozzi MC, Sandrolini F, Andreola F, Barbieri L, Lancellotti I, editors. Recycling electric arc furnace slag as unconventional component for building materials. Proceedings of 2nd International Conference on sustainable construction materials and technologies Ancona, Italy; 2010.
[27] Arribas I, Santamaría A, Ruiz E, Ortega-López V, Manso JM. Electric arc furnace slag and its use in hydraulic concrete. Construction and Building Materials. 2015;90:68-79.
[28] Choi S, Kim J-M, Han D, Kim J-H. Hydration properties of ladle furnace slag powder rapidly cooled by air. Construction and Building Materials. 2016;113:682-90.
[29] Coppola L, Buoso A, Coffetti D, Kara P, Lorenzi S. Electric arc furnace granulated slag for sustainable concrete. Construction and Building Materials. 2016;123:115-9.
[30] Singh S, Vashistha P, Chandra R, Rai AK. Study on leaching of electric arc furnace (EAF) slag for its sustainable applications as construction material. Process Safety and Environmental Protection. 2021;148:1315-26.
[31] Sun K, Peng X, Chu S, Wang S, Zeng L, Ji G. Utilization of BOF steel slag aggregate in metakaolin-based geopolymer. Construction and Building Materials. 2021;300:124024.
[32] Pan S-Y, Adhikari R, Chen Y-H, Li P, Chiang P-C. Integrated and innovative steel slag utilization for iron reclamation, green material production and CO2 fixation via accelerated carbonation. Journal of Cleaner Production. 2016;137:617-31.
[33] Ramadan M, Kohail M, Abadel AA, Alharbi YR, Tuladhar R, Mohsen A. De-aluminated metakaolin-cement composite modified with commercial titania as a new green building material for gamma-ray shielding applications. Case Studies in Construction Materials. 2022;17:e01344.
[34] Aderemi BO, Edomwonyi-Otu L, Adefila SS. A new approach to metakaolin dealumination. Australian Journal of Basic and Applied Sciences. 2009;3(3):2243-8.
[35] Muisa N, Nhapi I, Ruziwa W, Manyuchi MM. Utilization of alum sludge as adsorbent for phosphorus removal in municipal wastewater: A review. Journal of Water Process Engineering. 2020;35:101187.
[36] Abdelalim A, Ghorab H, Abdelaziz G, Elsayed M. DEALUMINATED KAOLIN AS A CEMENT REPLACEMENT MATERIAL. Journal cement Wapno Beton, 3rd issue, January. 2010.
[37] Mostafa N, El-Hemaly S, Al-Wakeel E, El-Korashy S, Brown P. Characterization and evaluation of the pozzolanic activity of Egyptian industrial by-products: I: Silica fume and dealuminated kaolin. Cement and Concrete Research. 2001;31(3):467-74.
[38] Prasetyoko D, Santoso M, Qoniah I, Leaw WL, Firda PB, Nur H. A review on synthesis of kaolin-based zeolite and the effect of impurities. Journal of the Chinese Chemical Society. 2020;67(6):911-36.
[39] Abo-El-Enein S, Heikal M, Amin M, Negm H. Reactivity of dealuminated kaolin and burnt kaolin using cement kiln dust or hydrated lime as activators. Construction and Building Materials. 2013;47:1451-60.
[40] Krivenko P, Guziy S. Fire resistant alkaline Portland cements. Proceedings of Alkali activated materials–research, production and utilization. 2007:333-47.
[41] Škvára F, Kopecký L, Myšková L, Šmilauer V, Alberovská L, Vinšová L. Aluminosilicate polymers–influence of elevated temperatures, efflorescence. Ceramics–Silikáty. 2009;53(4):276-82.
[42] Topcu IB, Toprak MU. Properties of geopolymer from circulating fluidized bed combustion coal bottom ash. Materials Science and Engineering: A. 2011;528(3):1472-7.
[43] Hussin M, Bhutta M, Azreen M, Ramadhansyah P, Mirza J. Performance of blended ash geopolymer concrete at elevated temperatures. Materials and Structures. 2015;48(3):709-20.
[44] Lahoti M, Tan KH, Yang E-H. A critical review of geopolymer properties for structural fire-resistance applications. Construction and Building Materials. 2019;221:514-26.
[45] Sakkas K, Nomikos P, Sofianos A, Panias D. Slag based geopolymer for passive fire protection of tunnels. Underground The Way to the Future—Informa UK Limited. 2013:343-9.

[46] Perera DS, Trautman RL. Geopolymers with the potential for use as refractory castables. Advances in Technology of Materials and Materials Processing Journal(ATM). 2005;7(2):187-90.
[47] Colangelo F, Cioffi R, Roviello G, Capasso I, Caputo D, Aprea P, et al. Thermal cycling stability of fly ash based geopolymer mortars. Composites part b: engineering. 2017;129:11-7.
[48] Varela B, Privorotskaya N, editors. The use of geopolymers as concrete coatings for fire protection. World Congress Geopolymers; 2005.
[49] C109/C109M-16a A. Standard test method for compressive strength of hydraulic cement mortars (using 2-in. or [50-mm] cube specimens). West Conshohocken: ASTM International. 2016.
[50] Heikal M, Nassar M, El-Sayed G, Ibrahim S. Physico-chemical, mechanical, microstructure and durability characteristics of alkali activated Egyptian slag. Construction and Building Materials. 2014;69:60-72.
[51] Heikal M, Morsy M, El-Shimy E, El-Enein S. Hydrothermal reactivity of granulated slag and sand using a lime-rich industrial waste as an activator. INDUSTRIA ITALIANA DEL CEMENTO. 2004:614-24.
[52] Zhang N, Wu L, Liu X, Zhang Y. Structural characteristics and cementitious behavior of basic oxygen furnace slag mud and electric arc furnace slag. Construction and Building Materials. 2019;219:11-8.
[53] Yip C, Van Deventer J. Microanalysis of calcium silicate hydrate gel formed within a geopolymeric binder. Journal of Materials Science. 2003;38(18):3851-60.
[54] Ramachandran VS, Paroli RM, Beaudoin JJ, Delgado AH. Handbook of thermal analysis of construction materials: William Andrew; 2002.